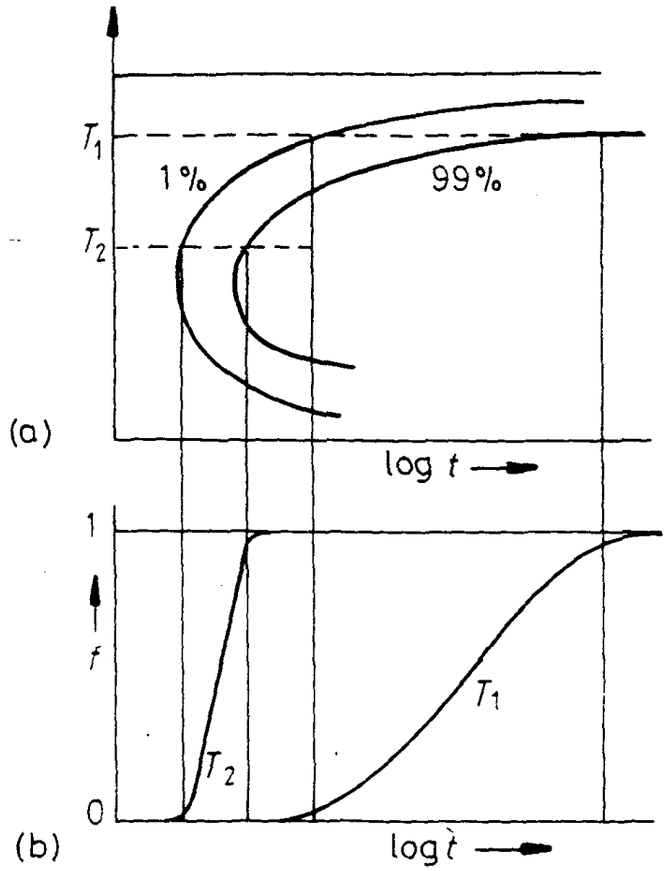

Fig. 5.23 The percentage transformation versus time for different transformation temperatures.

adjacent transformed volumes. Some of the problems involved are illustrated in Fig. 5.24. After quenching to the transformation temperature the metastable α phase will contain many nucleation sites (usually heterogeneous). One possible sequences of events, Fig. 5.24a, is that nuclei form throughout the transformation so that a wide range of particle sizes exists at any time. Another possibility is that all nuclei form right at the beginning of transformation, Fig. 5.24b. If all potential nucleation sites are consumed in the process this is known as *site saturation*. In Fig. 5.24a, f will depend on the nucleation rate and the growth rate. In Fig. 5.24b, f will only depend on the number of nucleation sites and the growth rate. For transformations of the type $\alpha \rightarrow \beta$ or $\alpha \rightarrow \beta + \gamma$ (known collectively as *cellular transformations*) all of the parent phase is consumed by the transformation product, Fig. 5.24c. In these cases the transformation does not terminate by the gradual reduction in the growth rate, but by the impingement of adjacent cells growing with a constant velocity. Pearlite, cellular precipitation, massive transformations and recrystallization belong to this category.

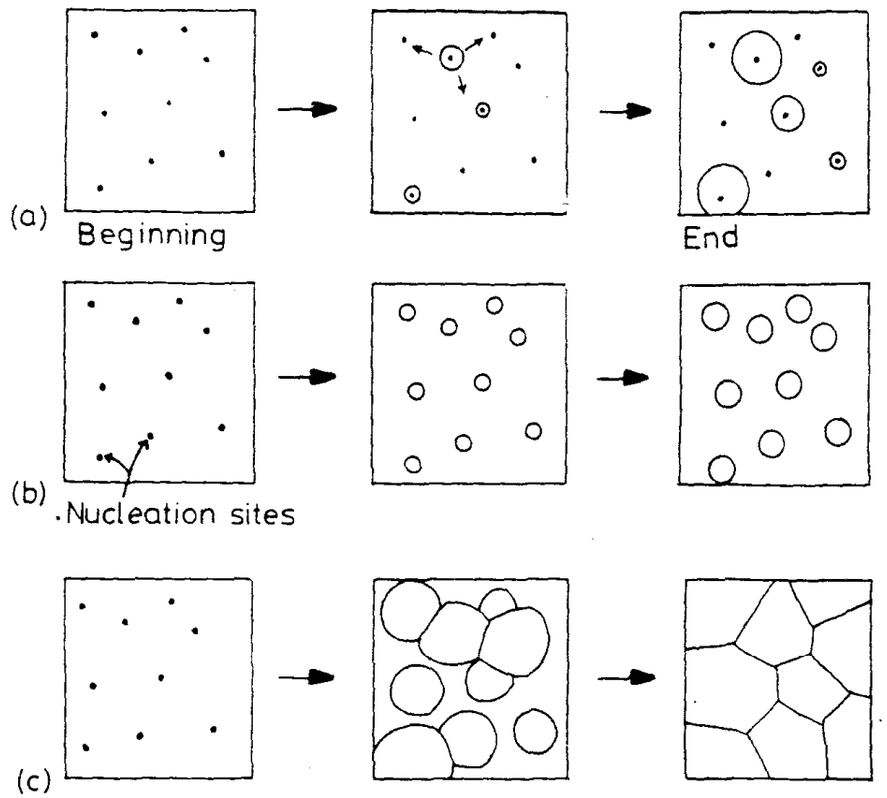

Fig. 5.24 (a) Nucleation at a constant rate during the whole transformation. (b) Site saturation—all nucleation occurs at the beginning of transformation. (c) A cellular transformation.

As a simple example of the derivation of $f(t, T)$ consider a cellular transformation ($\alpha \rightarrow \beta$) in which β cells are continuously nucleated throughout the transformation at a constant rate N^5. If the cells grow as spheres at a constant rate v, the volume of a cell nucleated at time zero will be given by

$$V = \frac{4}{3}\pi r^3 = \frac{4}{3}\pi(vt)^3$$

A cell which does not nucleate until time τ will have a volume

$$V' = \frac{4}{3}\pi v^3(t - \tau)^3$$

The number of nuclei that formed in a time increment of $d\tau$ will be $N d\tau$ per unit volume of untransformed α. Thus if the particles do not impinge on one another, for a unit total volume

$$f = \Sigma V' = \frac{4}{3}\pi N v^3 \int_0^t (t - \tau)^3 \, d\tau$$

i.e.

$$f = \frac{\pi}{3} N v^3 t^4 \tag{5.37}$$

This equation will only be valid for $f \ll 1$. As time passes the β cells will eventually impinge on one another and the rate of transformation will decrease again. The equation valid for randomly distributed nuclei for both long and short times is[6]

$$f = 1 - \exp\left(-\frac{\pi}{3} N v^3 t^4\right) \tag{5.38}$$

Note that this is the same as Equation 5.37 for short times, since $1 - \exp(-z) \simeq z$ when $z \ll 1$. It is also reasonable for long times since as $t \to \infty, f \to 1$.

Equation 5.38 is known as a *Johnson–Mehl–Avrami equation*. In general, depending on the assumptions made regarding the nucleation and growth processes, a variety of similar equations can be obtained with the form

$$f = 1 - \exp(-kt^n) \tag{5.39}$$

where n is a numerical exponent whose value can vary from ~1 to 4. Provided there is no change in the nucleation mechanism, n is independent of temperature. k, on the other hand, depends on the nucleation and growth rates and is therefore very sensitive to temperature. For example, in the case above, $k = \pi N v^3/3$ and both N and v are very temperature sensitive.

Since $\exp(-0.7) = 0.5$ the time for 50% transformation ($t_{0.5}$) is given by

$$kt_{0.5}^n = 0.7$$

i.e.

$$t_{0.5} = \frac{0.7^{1/n}}{k^{1/n}} \tag{5.40}$$

For the case discussed above

$$t_{0.5} = \frac{0.9}{N^{1/4} v^{3/4}} \tag{5.41}$$

Consequently it can be seen that rapid transformations are associated with large values of k, i.e. rapid nucleation and growth rates, as expected.

Civilian transformations that occur on cooling are typified by C-shaped TTT curves as shown in Fig. 5.23a. This can be explained on the basis of the variation of nucleation and growth rates with increasing undercooling. At temperatures close to T_e the driving force for transformation is very small so that both nucleation and subsequent growth rates are slow and a long time is required for transformation. When ΔT is very large, on the other hand, slow diffusion rates limit the rate of transformation. A maximum rate is, therefore, obtained at intermediate temperatures.

5.5 Precipitation in Age-Hardening Alloys

The theory of nucleation and growth that has been described above is able to provide general guidelines for understanding civilian transformations. Let us now turn to a consideration of some examples of the great variety of civilian transformations that can occur in solids, and begin with alloys that can be age-hardened. These alloys are characterized by phase diagrams such as that shown in Fig. 5.1a(i). Two extensively researched and illustrative examples are aluminium-copper and aluminium-silver alloys.

5.5.1 Precipitation in Aluminium-Copper Alloys

GP Zones

Figure 5.25 shows the Al-rich end of the Al–Cu phase diagram. If an alloy with the composition Al–4 wt% Cu (1.7 atomic %) is heated to a temperature of about 540 °C all copper will be in solid solution as a stable fcc α phase, and by quenching the specimen rapidly into water there is no time for any transformation to occur so that the solid solution is retained largely unchanged to room temperature. However, the solid solution is now supersaturated with Cu and there is a driving force for precipitation of the equilibrium θ phase, $CuAl_2$.

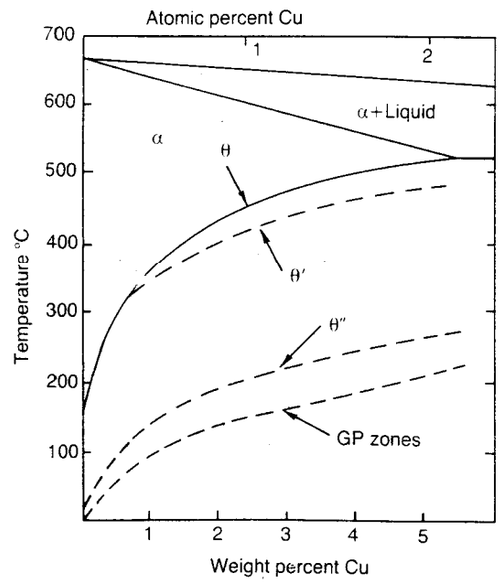

Fig. 5.25 Al–Cu phase diagram showing the metastable GP zone, θ″ and θ′ solvuses. (Reproduced from G. Lorimer, *Precipitation Processes in Solids*, K.C. Russell and H.I. Aaronson (Eds.), The Metallurgical Society of AMIE, 1978, p. 87.)

If the alloy is now *aged* by holding for a period of time at room temperature or some other temperature below about 180 °C it is found that the first precipitate to nucleate is not θ but coherent Cu-rich GP zones. (Copper-rich zones in Al–Cu alloys were detected independently in 1938 by Guinier and Preston from streaks in X-ray diffraction patterns.) The reason for this can be understood on the basis of the relative activation energy barriers for nucleation as discussed earlier. GP zones are fully coherent with the matrix and therefore have a very low interfacial energy, whereas the θ phase has a complex tetragonal crystal structure which can only form with high-energy incoherent interfaces. In addition, the zones minimize their strain energy by choosing a disc-shape perpendicular to the elastically soft ⟨100⟩ directions in the fcc matrix, Fig. 5.26. Therefore, despite the fact that the driving force for precipitation of GP zones ($\Delta G_v - \Delta G_s$) is less than for the equilibrium phase, the barrier to nucleation (ΔG^*) is still less, and the zones nucleate most rapidly. The microstructure of an Al–Cu alloy aged to produce GP zones is shown in Fig. 5.30a. These zones are about 2 atomic layers thick and 10 nm in diameter with a spacing of ~10 nm. The zones themselves are not resolved. The contrast in the image is due to the coherency misfit strain perpendicular to the zones. This distorts the lattice causing local variations in the intensity of electron diffraction, which in turn shows up as variations in the image intensity. Microstructurally, the zones appear to be homogeneously nucleated, however excess vacancies are thought to play an important role in their formation. This point will be returned to later.

GP zones are formed as the first precipitate during low-temperature ageing of many technologically important alloys, notably those based on aluminium (see Tables 5.2 and 5.3). In dilute Al–Zn and Al–Ag alloys Zn-rich and Ag-rich GP zones are found. In these cases there is very little misfit strain and ΔG^* is minimized by the formation of spherical zones with a minimum interfacial energy, Fig. 3.39.

Transition Phases

The formation of GP zones is usually followed by the precipitation of so-called transition phases. In the case of Al–Cu alloys the equilibrium θ phase is

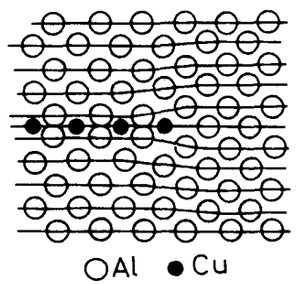

Fig. 5.26 Section through a GP zone parallel to the (200) plane. (Based on the work of V. Gerold: *Zeitschrift für Metallkunde* **45** (1954) 599.)

Table 5.2 Some Precipitation-Hardening Sequences

(Mainly from J.W. Martin, *Precipitation Hardening*, Pergamon Press, Oxford, 1968.)

Base metal	Alloy	Precipitation sequence
Aluminium	Al–Ag	GPZ (spheres) → γ′ (plates) → γ (Ag_2Al)
	Al–Cu	GPZ (discs) → θ″ (discs) → θ′ (plates) → θ ($CuAl_2$)
	Al–Cu–Mg	GPZ (rods) → S′ (laths) → S ($CuMgAl_2$) (laths)
	Al–Zn–Mg	GPZ (spheres) → η′ (plates) → η ($MgZn_2$) (plates or rods)
	Al–Mg–Si	GPZ (rods) → β′ (rods) → β(Mg_2Si) (plates)
Copper	Cu–Be	GPZ (discs) → γ′ → γ (CuBe)
	Cu–Co	GPZ (spheres) → β (Co) (plates)
Iron	Fe–C	ε-carbide (discs) → Fe_3C (plates)
	Fe–N	α″ (discs) → Fe_4N
Nickel	Ni–Cr–Ti–Al	γ′ (cubes or spheres)

preceded by θ″ and θ′. The total precipitation process can be written

$$\alpha_0 \rightarrow \alpha_1 + \text{GP zones} \rightarrow \alpha_2 + \theta'' \rightarrow \alpha_3 + \theta' \rightarrow \alpha_4 + \theta$$

where α_0 is the original supersaturated solid solution, α_1 is the composition of the matrix in equilibrium with GP zones, α_2 the composition in equilibrium with θ″ etc.

Figure 5.27 shows a schematic free energy diagram for the above phases. Since GP zones and the matrix have the same crystal structure they lie on the same free energy curve (ignoring strain energy effects—see Section 5.5.5). The transition phases θ″ and θ′ are less stable than the equilibrium θ phase and consequently have higher free energies as shown. The compositions of the matrix in equilibrium with each phase—α_1, α_2, α_3, α_4—are given by the common tangent construction. These compositions correspond to points on the solvus lines for GP zones, θ″, θ′ and θ shown in Fig. 5.25. The free energy of the alloy undergoing the above precipitation sequence decreases as

$$G_0 \rightarrow G_1 \rightarrow G_2 \rightarrow G_3 \rightarrow G_4$$

as shown in Fig. 5.27. Transformation stops when the minimum free energy equilibrium state G_4 is reached, i.e. $\alpha_4 + \theta$.

Transition phases form because, like GP zones, they have a lower activation energy barrier for nucleation than the equilibrium phase, Fig. 5.28a. The free energy of the alloy therefore decreases more rapidly via the transition phases than by direct transformation to the equilibrium phase, Fig. 5.28b.

Table 5.3 Mechanical Properties of some Commercial Precipitation-Hardening Alloys

Base metal	Alloy	Composition (wt%)	Precipitate	YS* MPA	UTS* MPa	Elongation* %
Aluminium	2024	Cu (4.5) Mg (1.5) Mn (0.6)	S′ (Al_2CuMg)	390	500	13
	6061	Mg (1.0) Si (0.6) Cu (0.25) Cr (0.2)	β′ (Mg_2Si)	280	315	12
	7075	Zn (5.6) Mg(2.5) Cu (1.6) Mn (0.2) Cr (0.3)	η′ ($MgZn_2$)	500	570	11
Copper	Cu–Be	Be (1.9) Co (0.5)	zones	770	1160	5
Nickel	Nimonic 105	Co (20) Cr (15) Mo (5) Al (4.5) Ti (1.0) C (0.15)	γ′ (Ni_3TiAl)	750†	1100†	25†
Iron	Maraging Steel	Ni (18) Co (9) Mo (5) Ti (0.7) Al (0.1)	σ (FeMo) +Ni_3Ti	1000	1900	4

* At peak hardness tested at room temperature.
† Tested at 600 °C.

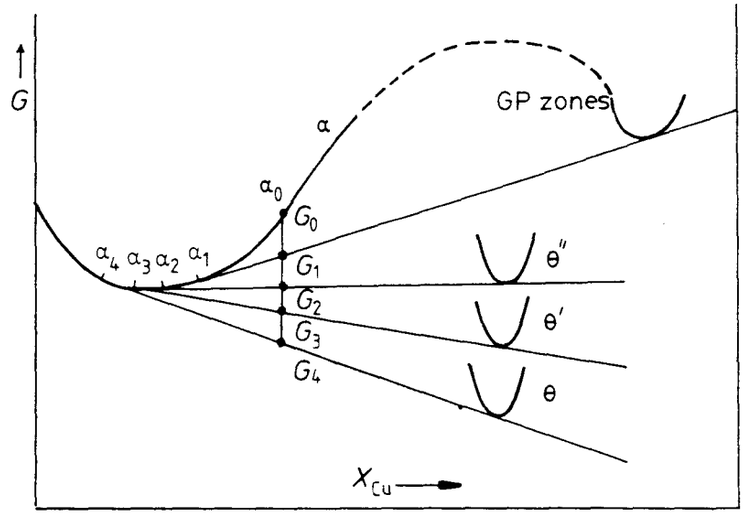

Fig. 5.27 A schematic molar free energy diagram for the Al–Cu system.

The lower activation energy barriers are achieved because the crystal structures of the transition phases are intermediate between those of the matrix and the equilibrium phase. In this way the transition phases can achieve a high degree of coherence and thus a low interfacial energy contribution to ΔG^*. The equilibrium phase on the other hand usually has a complex crystal structure that is incompatible with the matrix and results in high-energy interfaces and high ΔG^*.

The crystal structures of θ″, θ′ and θ are shown in Fig. 5.29 along with that of the fcc matrix for comparison. θ″ has a tetragonal unit cell which is essentially a distorted fcc structure in which the copper and aluminium atoms are ordered on (001) planes as shown. Note that the atomic structure of the (001) planes is identical to that in the matrix, and the (010) and (100) planes are very similar, apart from a small distortion in the [001] direction. θ″ forms as fully coherent plate-like precipitates with a $\{001\}_\alpha$ habit plane and the following orientation relationship to the matrix:

$$(001)_{\theta''} \| (001)_\alpha$$
$$[100]_{\theta''} \| [100]_\alpha$$

A high magnification transmission electron micrograph of an alloy aged to produce θ″ precipitates is shown in Fig. 5.30b. Like the GP zones in Fig. 5.30a, the θ″ precipitates are visible by virtue of the coherency-strain fields caused by the misfit perpendicular to the plates. θ″ precipitates are larger than GP zones being up to ~10 nm thick and 100 nm in diameter.

θ′ is also tetragonal with an approximate composition $CuAl_2$ and again has (001) planes that are identical with $\{001\}_\alpha$. The (100) and (010) planes,

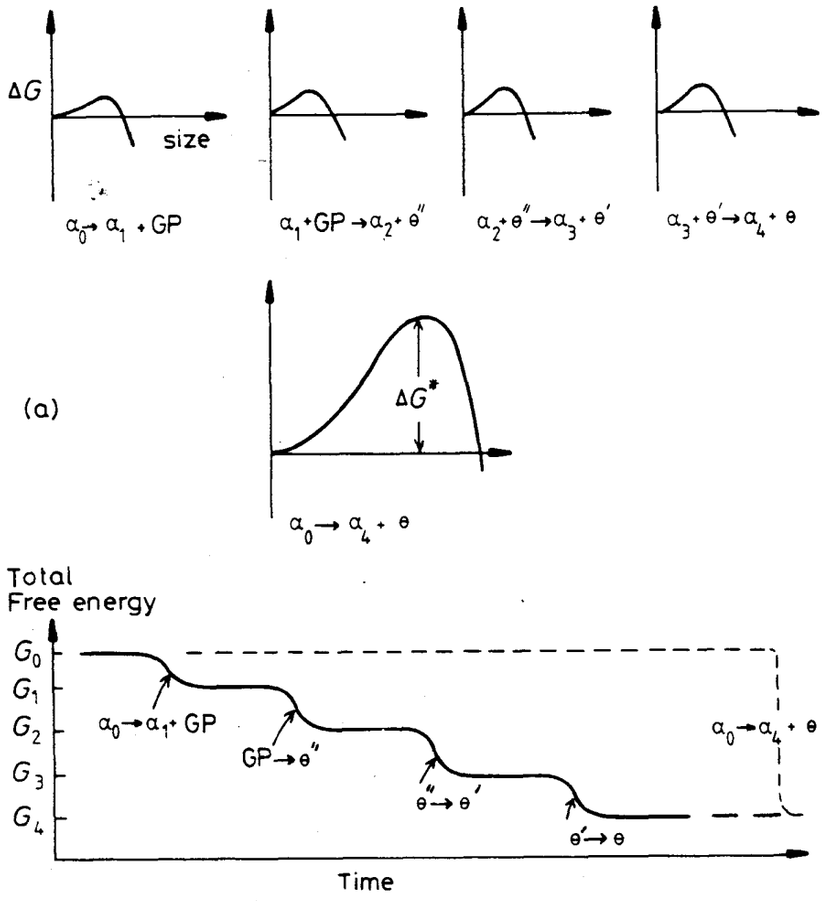

Fig. 5.28 (a) The activation energy barrier to the formation of each transition phase is very small in comparison to the barrier against the direct precipitation of the equilibrium phase. (b) Schematic diagram showing the total free energy of the alloy v. time.

however, have a different crystal structure to the matrix and a large misfit in the [001] direction. θ′ therefore forms as plates on $\{001\}_\alpha$ with the same orientation relationship as θ″. The broad faces of the plates are initially fully coherent but lose coherency as the plates grow, while the edges of the plates are either incoherent or have a complex semicoherent structure. A transmission electron micrograph of θ′ plates ~1 μm diameter is shown in Fig. 5.30c. Note the presence of misfit dislocations in the broad faces of the precipitates.

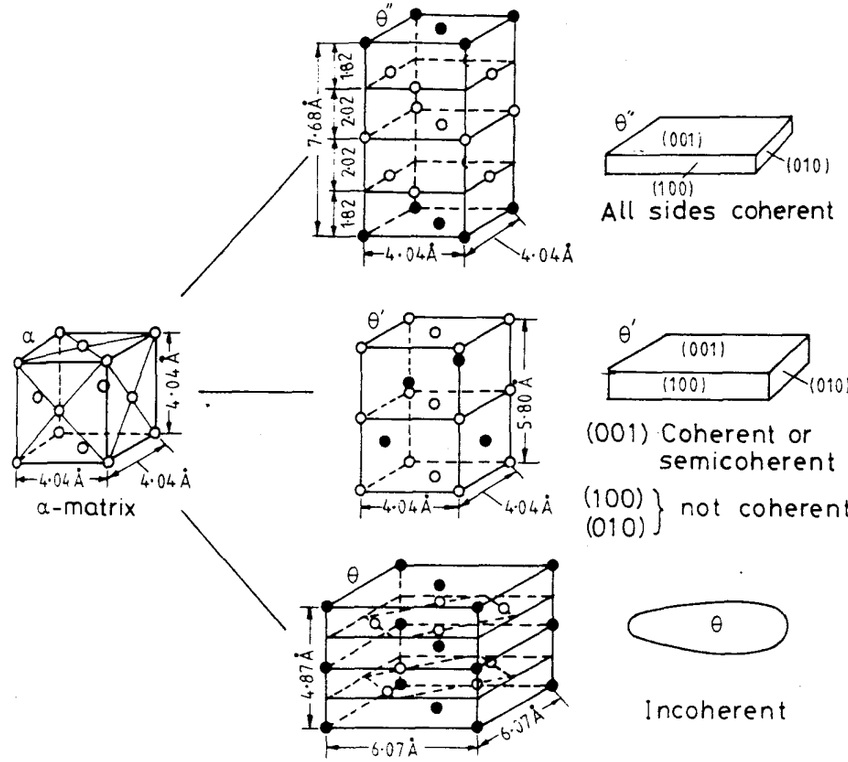

Fig. 5.29 Structure and morphology of θ″, θ′ and θ in Al–Cu (○ Al, ● Cu).

Note also that since the edges of the plates are not coherent there are no long-range coherency-strain fields.

The equilibrium θ phase has the approximate composition $CuAl_2$ and a complex body-centred tetragonal structure as shown in Fig. 5.29. There are no planes of good matching with the matrix and only incoherent, or at best complex semicoherent interfaces are possible. The microstructure at this final stage of ageing is shown in Fig. 5.30d. Note the large size and coarse distribution of the precipitates.

The transformation from GP zones to θ′ occurs by the *in situ* transformation of the zones, which can be considered as very potent nucleation sites for θ″. After longer ageing times the θ′ phase nucleates on matrix dislocations with two orientations of θ′ plates on any one $\frac{a}{2}\langle 110\rangle$ dislocation. This is because the strain field of such a dislocation is able to reduce the misfit in two ⟨100⟩ matrix directions. Figure 5.31a shows θ′ plates that have nucleated on dislocations. Note that as the θ′ grows the surrounding, less-stable θ″ can be seen to dissolve. After still longer ageing times the equilibrium θ phase

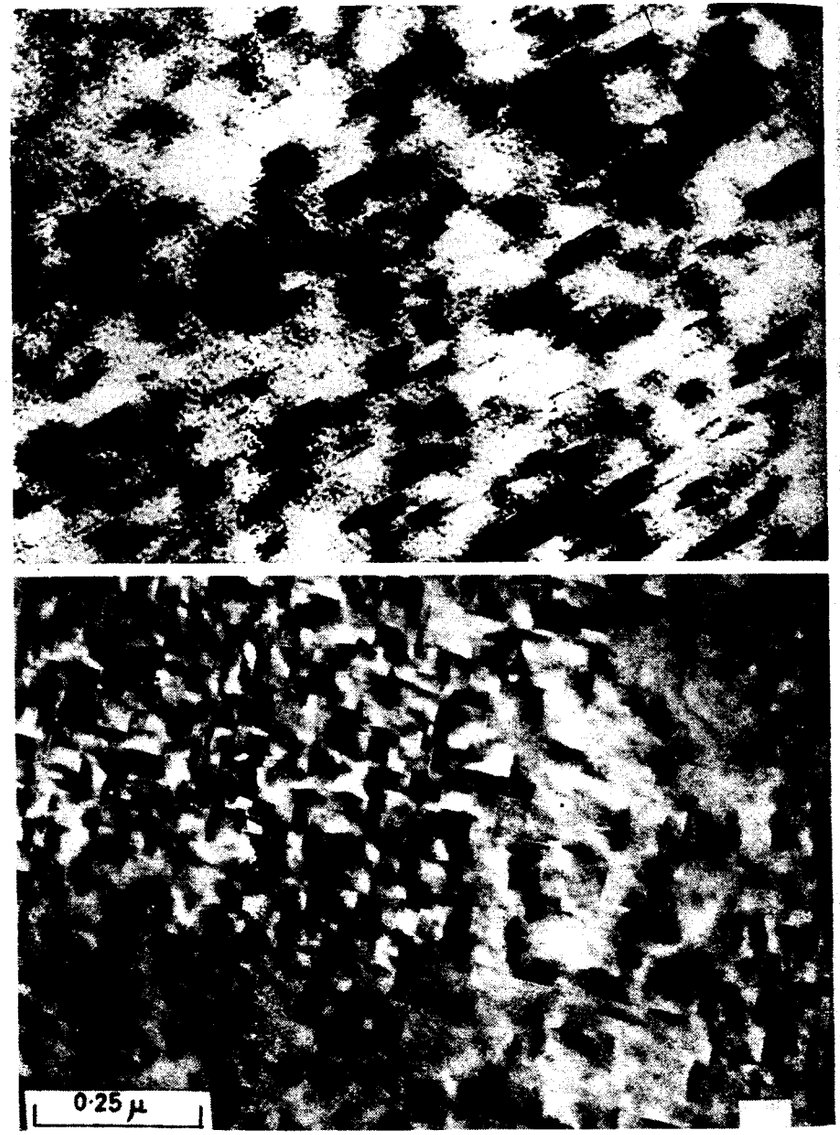

Fig. 5.30 Microstructures at different stages during ageing of Al–Cu alloys. (a) GP zones × 720 000. (b) θ″ × 63 000. (c) θ′ × 18 000. (d) θ × 8000. [(a) After R.B. Nicholson and J. Nutting. *Philosophical Magazine* **3** (1958) 531. (b) R.B. Nicholson, G. Thomas and J. Nutting. *Journal of the Institute of Metals* **87** (1958–1959) 431. (c) G.C. Weatherly and R.B. Nicholson. *Philosophical Magazine* **17** (1968) 813. (d) G.A. Chadwick. *Metallography of Phase Transformations*, Butterworths, London, 1972, from C. Laird.]

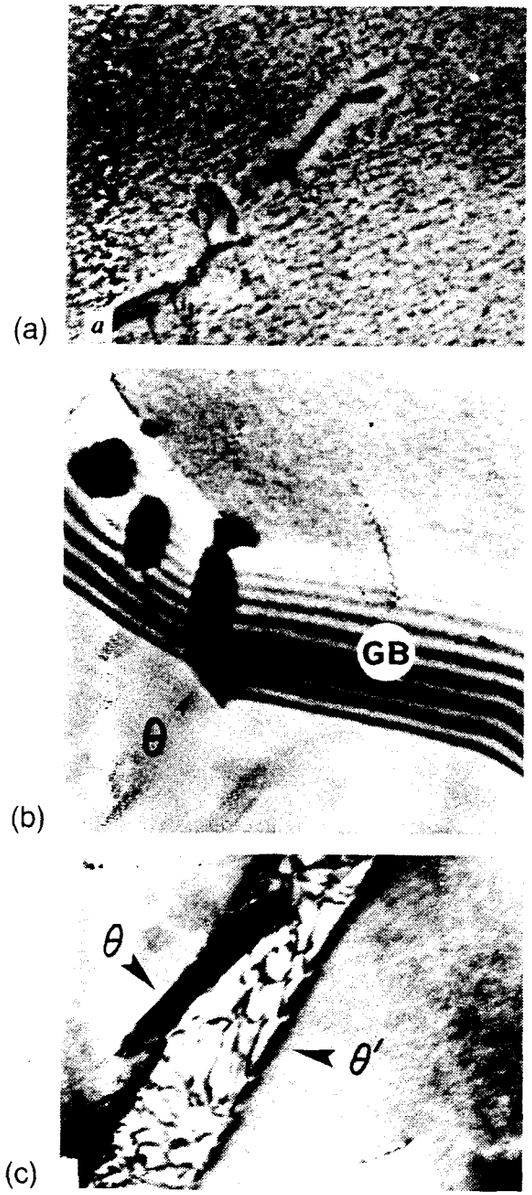

Fig. 5.31 Electron micrographs showing nucleation sites in Al–Cu alloys. (a) $\theta'' \rightarrow \theta'$. θ' nucleates at dislocation (× 70 000). (b) θ nucleation on grain boundary (GB) (× 56 000). (c) $\theta' \rightarrow \theta$. θ nucleates at θ'/ matrix interface (× 70 000). (After P. Haasen, *Physical Metallurgy*, Cambridge University Press, Cambridge, 1978.)

nucleates either on grain boundaries, Fig. 5.31b, or at θ'/matrix interfaces, Fig. 5.31c. The choice of these nucleation sites is governed by the need to reduce the large interfacial energy contribution to ΔG^* for this phase.

The full sequence of GP zones and transition precipitates is only possible when the alloy is aged at a temperature below the GP zones solvus. For example, if ageing is carried out at a temperature above the θ'' solvus but below the θ' solvus, Fig. 5.25, the first precipitate will be θ', heterogeneously nucleated on dislocations. If ageing is carried out above the θ' solvus, the only precipitate that is possible is θ which nucleates and grows at grain boundaries. Also, if an alloy containing GP zones is heated to above the GP zone solvus the zones will dissolve. This is known as *reversion*.

The effect of ageing temperature on the sequence of precipitates is illustrated by a schematic TTT diagram in Fig. 5.32. The fastest transformation rates are associated with the highest nucleation rates and therefore the finest precipitate distributions. There is consequently an increasing coarseness of microstructure through the sequence of precipitates as can be seen in Fig. 5.30.

The mechanism whereby a more stable precipitate grows at the expense of a less stable precipitate is illustrated in Fig. 5.33 for the case θ''/θ'. Figure 5.27 shows that the Cu concentration in the matrix close to the θ'' precipitates (α_2) will be higher than that close to $\theta'(\alpha_3)$. Therefore Cu will tend to diffuse through the matrix away from θ'', which thereby dissolves, and towards θ', which grows.

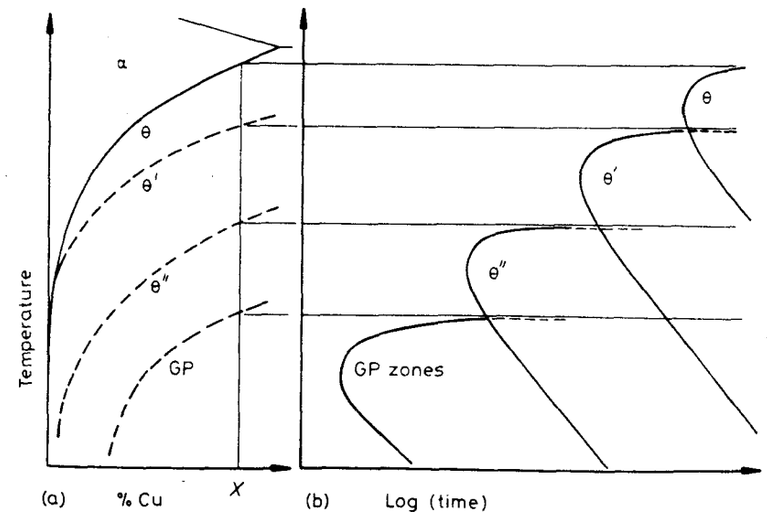

Fig. 5.32 (a) Metastable solvus lines in Al–Cu (schematic). (b) Time for start of precipitation at different temperatures for alloy X in (a).

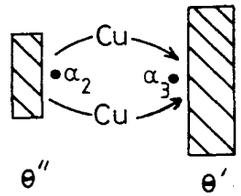

Fig. 5.33 Matrix in equilibrium with θ″ (α_2) contains more Cu than matrix in equilibrium with θ′ (α_3). Cu diffuses as shown causing θ″ to shrink and θ′ to grow.

5.5.2 *Precipitation in Aluminium–Silver Alloys*

Figure 5.34 shows the Al–Ag phase diagram. If alloys containing up to about 23 atomic % Ag are solution treated, quenched and given a low-temperature ageing treatment the precipitation sequence is

$$\alpha_0 \rightarrow \alpha_1 + \text{GP zones} \rightarrow \alpha_2 + \gamma' \rightarrow \alpha_3 + \gamma$$

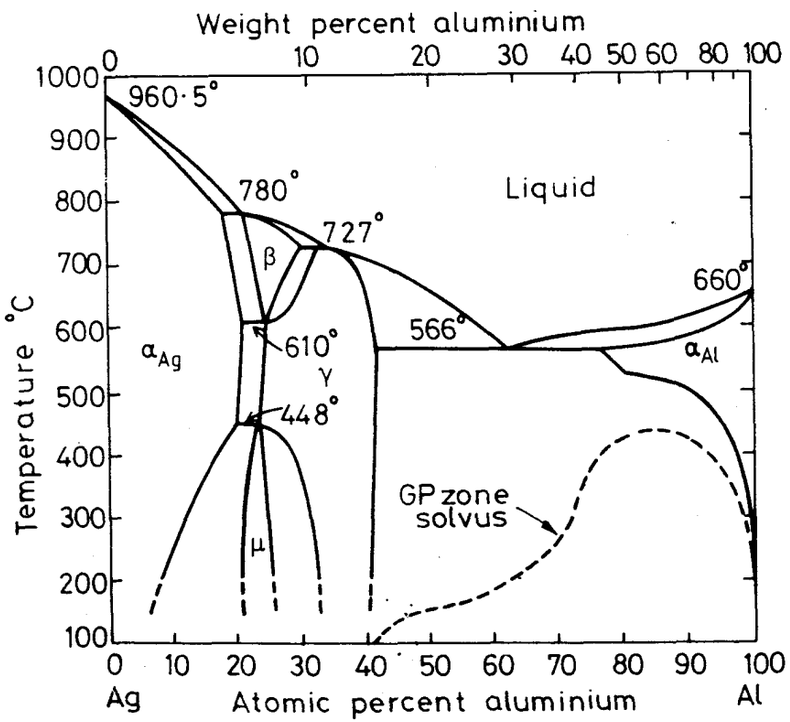

Fig. 5.34 Al–Ag phase diagram showing metastable two-phase field corresponding to GP zones. (After R. Baur and V. Gerold, *Zeitschrift für Metallkunde* **52** (1961) 671.)

As discussed earlier, the GP zones in this system are spherical. γ′ is a close-packed hexagonal transition phase with an orientation relationship to the matrix of

$$(0001)_{\gamma'}//(111)_{\alpha}$$
$$[11\bar{2}0]_{\gamma'}//[1\bar{1}0]_{\alpha}$$

γ′ is heterogeneously nucleated on helical dislocations by the enrichment of stacking faults with silver as discussed in Section 5.2. The equilibrium γ phase has the composition Ag_2Al, is hexagonal and has the same orientation relationship with the matrix as γ′. It forms as plate-like precipitates with (111) habit planes. γ can be formed from γ′ by the latter acquiring misfit dislocations. It can also be separately nucleated at grain boundaries and grow by a cellular mechanism (see Section 5.7).

5.5.3 *Quenched-in Vacancies*

It was shown in Chapter 1 that the equilibrium concentration of vacancies increases exponentially with temperature. Thus the *equilibrium* vacancy concentration will be relatively high at the solution treatment temperature and much lower at the ageing temperature. However, when the alloy is rapidly quenched from the high temperature there will be no time for the new equilibrium concentration to be established and the high vacancy concentration becomes *quenched-in*. Given time, those vacancies in excess of the equilibrium concentration will *anneal out*. There will be a tendency for vacancies to be attracted together into *vacancy clusters*, and some clusters collapse into dislocation loops which can grow by absorbing more vacancies. The dislocations that are already present can also absorb vacancies by *climbing*. In this way straight screw dislocations can become converted into longer helical edge dislocations. There are many ways, therefore, in which excess vacancies are able to provide heterogeneous nucleation sites.

Another effect of quenched-in vacancies is to greatly increase the rate at which atoms can diffuse at the ageing temperatures. This in turn speeds up the process of nucleation and growth. Indeed the only way of explaining the rapid formation of GP zones at the relatively low ageing temperatures used is by the presence of excess vacancies.

If GP zones are separated by a mean spacing λ, the mean diffusion distance for the solute atoms is λ/2. Therefore, if the zones are observed to form in a time t, the effective diffusion coefficient is roughly given by x^2/t, i.e.

$$D \simeq \frac{\lambda^2}{4t}$$

If high-temperature diffusion data are extrapolated down to the ageing temperature, the values obtained are orders of magnitude smaller than the above value. The difference can, however, be explained by a quenched-in